Enhancement of Electrocatalytic Activity as a Function of Structural Order in Perovskite Oxides

Surendra B. Karki[a,‖], Ram Krishna Hona[a,§,‖], Ming Yu[b], Farshid Ramezanipour[a,*]

[a]Department of Chemistry, University of Louisville, Louisville, Kentucky 40292, USA
[§]Current address: Department of Tribal Environmental Science, United Tribes Technical College, Bismarck, ND, USA
[b]Department of Physics and Astronomy, University of Louisville, Louisville, KY 40292, USA
‖ These authors contributed equally to this work
*Corresponding author. Email: farshid.ramezanipour@louisville.edu, Phone: (502) 852-7061

Supporting Information Placeholder

ABSTRACT: Electrocatalytic splitting of water is a promising method of hydrogen generation. Here, we report an enhanced electrocatalytic performance for water electrolysis, achieved through a progressive increase in the ordering of oxygen-vacancies in the structural network of oxides. In transition from $Sr_2FeCoO_{6-\delta}$ (disordered) to $CaSrFeCoO_{6-\delta}$ (ordered) and $Ca_2FeCoO_{6-\delta}$ (highly ordered), the change in the average ionic radius of the A-site metals leads to an increase in the concentration and ordering of oxygen-vacancies, resulting in a progressive enhancement of the electrocatalytic activity for both cathodic and anodic half-reactions of water-splitting, i.e., hydrogen-evolution (HER) and oxygen-evolution (OER) reactions. The OER electrocatalysis is particularly important, as it is considered the bottleneck for water electrolysis. These electrocatalysts show better activity than the precious metal catalyst RuO_2. Contrary to most bifunctional catalysts reported to date, these catalysts can be used in bulk form, without the need for nanofabrication, composite formation, or any additional processing. Density functional theory calculations indicate that the vacancy-order leads to a shift of the electronic bands toward the Fermi level. We propose that the ordering of oxygen-vacancies can be used as a handle for the design of highly active electrocatalysts.

Keywords: Electrocatalyst, Water-splitting, Perovskite oxide, Oxygen-vacancies, Ordering

Efficient and sustainable electrocatalysts that can replace the precious metal catalysts in electrochemical processes are highly desired. Of particular interest are the two half reactions of water electrolysis, namely hydrogen-evolution (HER) and oxygen-evolution (OER) reactions. The latter is considered as the bottleneck for water electrolysis and is essential to the operation of metal-air batteries and regenerative fuel cells. Among various materials that have been explored as electrocatalysts for these reactions, transition metal oxides with perovskite-type structure have shown great promise. These materials have the general formula ABO_3 (Figure 1a), where A is often a lanthanide or alkaline-earth metal, and B is usually a transition metal. One well-known example is $Ba_{0.5}Sr_{0.5}Co_{0.8}Fe_{0.2}O_{3-\delta}$ (BSCF), which has an electrocatalytic activity comparable to some precious metal OER catalysts.[1] Other examples include $SrNb_{0.1}Co_{0.7}Fe_{0.2}O_{3-\delta}$,[2] $SrCo_{0.9}Ti_{0.1}O_{3-\delta}$,[3] $La_{0.5}Sr_{0.5}Co_{0.8}Fe_{0.2}O_{3-\delta}$,[4] and $La_{0.7}(Ba_{0.5}Sr_{0.5})_{0.3}Co_{0.8}Fe_{0.2}O_{3-\delta}$.[5] There have also been studies on the HER activity of perovskite-type oxides, such as $Pr_{0.5}(Ba_{0.5}Sr_{0.5})_{0.5}Co_{0.8}Fe_{0.2}O_{3-\delta}$[6] and $SrNb_{0.1}Co_{0.7}Fe_{0.2}O_{3-\delta}$.[7]

We have recently studied a wide range of perovskite-based oxides for both OER and HER,[8, 9] where the focus has been on creating oxygen-vacancies in perovskite oxides in order to enhance their electrocatalytic properties. The oxygen-deficient perovskites, $ABO_{3-\delta}$ (or $A_2B_2O_{6-\delta}$), often contain random distribution of oxygen-vacancies, where the overall perovskite framework is maintained but some oxygen sites are vacant, as is the case in some of the catalysts mentioned above.[1-7]

However, it is also possible to synthesize perovskite-based oxides, where the oxygen-vacancies have an ordered distribution, leading to an ordered arrangement of tetrahedral or square-pyramidal units, as opposed to the typical octahedral coordination observed in a regular perovskite system.[8, 9] Among such materials, we recently utilized X-ray and neutron diffraction to study the crystal structure of the series $Sr_2FeCoO_{6-\delta}$, $CaSrFeCoO_{6-\delta}$ and $Ca_2FeCoO_{6-\delta}$,[10] which show a methodical increase in the ordering of oxygen-vaccines. In the present work, we demonstrate a remarkable finding, where the electrocatalytic activity for both HER and OER is systematically enhanced as a function of vacancy-order. In particular, the ordering of vacancies leads to a catalyst which is by far superior to precious metal catalysts, such as RuO_2. Furthermore, the remarkably high intrinsic activity of this catalyst enables it to catalyze the HER and OER in bulk form, without the need for elaborate nanofabrication or composite formation.

All three materials are synthesized under the same conditions, as described in the Supporting Information. Iodometric titrations show that the degree of oxygen-deficiency is $\delta = 0.5$ for $Sr_2FeCoO_{6-\delta}$, $\delta = 0.8$ for $CaSrFeCoO_{6-\delta}$, and $\delta = 1.0$ for $Ca_2FeCoO_{6-\delta}$. Rietveld refinements (Figure S1a) using X-ray diffraction data confirm that the structure of $Sr_2FeCoO_{6-\delta}$ resembles that of a typical perovskite with octahedral coordination around

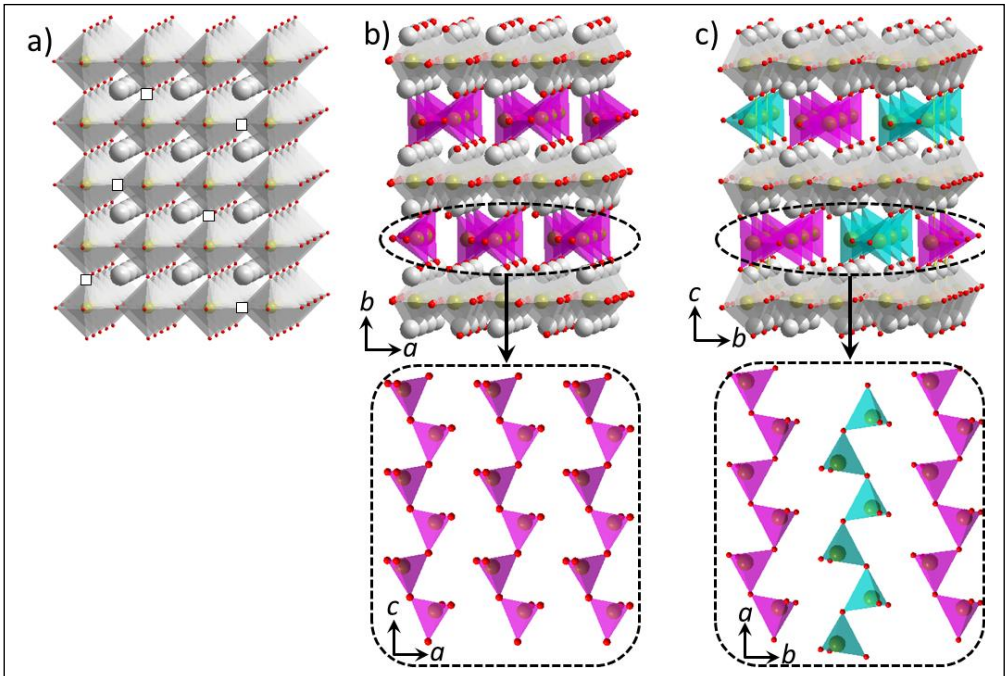

Figure 1. (a) Structure of $Sr_2FeCoO_{6-\delta}$, containing a random distribution of oxygen-vacancies, represented by white squares. (b) and (c) show $CaSrFeCoO_{6-\delta}$ and $Ca_2FeCoO_{6-\delta}$, respectively, where oxygen-vacancies only appear in every other layer. Dotted panels show the top view of the orientation of tetrahedral chains that form due to oxygen-vacancies.

transition metals (Figure 1a).[10] The vacant oxygen sites are distributed randomly, as required by the cubic perovskite structure, which contains one crystallographic position for the A-site, one for the B-site metal, and one for oxygen.

However, the decrease in the average ionic radius of the A-site, by incorporation of calcium, leads to an ordered structure in $CaSrFeCoO_{6-\delta}$. The structure and Rietveld refinement profile are shown in Figures 1b and S1b, respectively.[10] In this structure, the oxygen-vacancies are present in every other layer, lowering the coordination number of the B-site metals from 6 to 4. This leads to the formation of $(Fe/Co)O_4$ tetrahedral units in every other layer (purple polyhedra in Figures 1b). The remaining layers (grey polyhedra in Figures 1b) do not have oxygen vacancies and retain the typical octahedral coordination of a perovskite structure. The connectivity of all polyhedra is through corner-sharing. The tetrahedral $(Fe/Co)O_4$ units are connected to form chains that are sandwiched between the octahedral layers. All tetrahedral chains have the same orientation, as observed in Figures 1b.

An even higher degree of order can be attained when the average ionic radius of the A-site is decreased further to form $Ca_2FeCoO_{6-\delta}$.[10] In this material, the oxygen-vacancies are ordered, and occur only in every other layer, forming 4-coordinated tetrahedral units similar to the above structure. However, there is an additional degree of order, where the tetrahedral chains that form due to the oxygen vacancies, have alternating orientations (Figures 1c), forming an R-L-R-L-… arrangement (R = right handed; L = left handed).

Therefore, there is a methodical increase in the ordering of oxygen-vacancies from $Sr_2FeCoO_{6-\delta}$ (disordered) to $CaSrFeCoO_{6-\delta}$ (ordered) and $Ca_2FeCoO_{6-\delta}$ (highly ordered). These changes correlate directly with electrocatalytic properties. The HER overpotential at 10 mA/cm^2 (η_{10})[2, 11, 12] for the disordered material $Sr_2FeCoO_{6-\delta}$ is 490 mV in 1 M KOH, which is lowered to η_{10} = 390 mV for the vacancy-ordered material $CaSrFeCoO_{6-\delta}$. Further lowering of the overpotential is observed for the highly ordered material $Ca_2FeCoO_{6-\delta}$, η_{10} = 250 mV (Figure 2a). The latter material shows better electrocatalytic activity than some reported perovskite oxides such as $Ba_{0.5}Sr_{0.5}Co_{0.8}Fe_{0.2}O_{3-\delta}$ (η_{10} = 430 mV),[13] $La_{0.96}Ce_{0.04}CoO_{3-\delta}$ (η_{10} = 305 mV),[14] $NdBaMn_2O_{6-\delta}$ (η_{10} = 290 mV),[15] and $SrNb_{0.1}Co_{0.7}Fe_{0.2}O_{3-\delta}$ nanorods (262 mV).[7] There is also a methodical enhancement of the HER kinetics as a function of the structural order, as evident from the slopes of Tafel plots, η vs log j (Figure 2b).[16, 17] The decrease in Tafel slope correlates with the increase in structural order, indicating faster charge-transfer and enhanced kinetics for the ordered materials.[18, 19] Furthermore, the enhanced charge-transfer is evident from the systematic decrease in the charge-transfer resistance in impedance spectroscopy data in the HER region,[15] which matches the trend in structural order, as shown in Figure 2c. The best catalyst, $Ca_2FeCoO_{6-\delta}$, maintains its high activity for at least 2000 cycles, as demonstrated in Figure 2d.

The correlation between the electrocatalytic activity and vacancy-order is also observed for the OER electrocatalysis, as evident from the overpotential values (η_{10}) beyond the thermodynamic potential of 1.23 V at 10 mA/cm^2. The disordered material, $Sr_2FeCoO_{6-\delta}$, shows an overpotential of η_{10} = 280 mV in 1 M KOH, which is lowered to η_{10} = 270 mV for the vacancy-ordered material $CaSrFeCoO_{6-\delta}$, and η_{10} = 250 mV for the highly ordered $Ca_2FeCoO_{6-\delta}$. This is a remarkably low overpotential for a single-phase bulk oxide, based on non-noble metals. It is by far superior to that of the noble metal catalyst RuO_2,[20-22] as shown in Figure 3a. The vast majority of the previously reported oxide electrocatalysts show an OER overpotential of η_{10} > 300 mV, such as $La_{0.6}Sr_{0.4}Co_{0.8}Fe_{0.1}Mn_{0.1}O_3$ (343 mV),[23] $PrBaCo_2O_{5.75}$ (360 mV),[24] $PrBa_{0.25}Sr_{0.75}Co_2O_{5.95}$ (420 mV),[25] and $Pr_{0.5}Ba_{0.5}Co_{0.8}W_{0.2}O_{3-\delta}$ (325 mV).[26]

In addition, the vacancy-ordered $Ca_2FeCoO_{6-\delta}$ has a unique property, which is its ability to act as a highly active electrocatalyst without the need for nanofabrication, composite formation, or any additional processing. It does not even need the addition of carbon black, which is routinely added to catalysts for OER/HER, indicating its superior intrinsic activity. The few existing oxide catalysts that show such high level of OER activity, often require elaborate nanofabrication processes or multicomponent composite formation. For example, an OER overpotential of η_{10} = 297 mV has been observed for Co_3O_4/Co-Fe oxide double-shelled nanoboxes, obtained using a multi-step process involving metal-organic frameworks.[27] Also an overpotential of η_{10} = 240 mV is reported for 3D hybrid porous $CoFe_2O_4$/C nanorod arrays supported on nickel

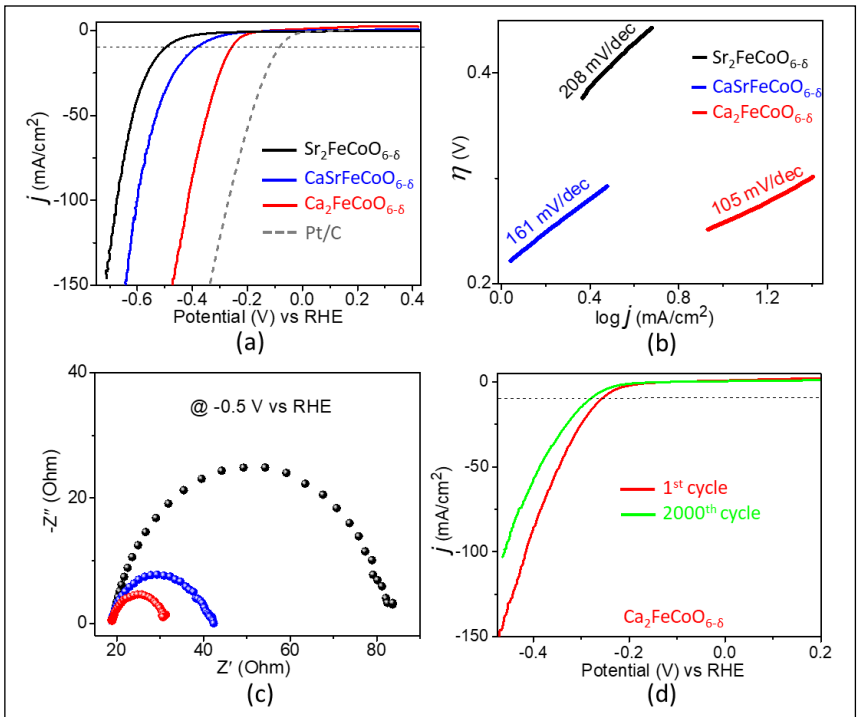

Figure 2. (a) HER polarization curves in 1M KOH. (b) Tafel plots and slopes. (c) Impedance spectroscopy data indicating the charge transfer resistance in the HER region. (d) Polarization curve for $Ca_2FeCoO_{6-\delta}$ after 2000 cycles.

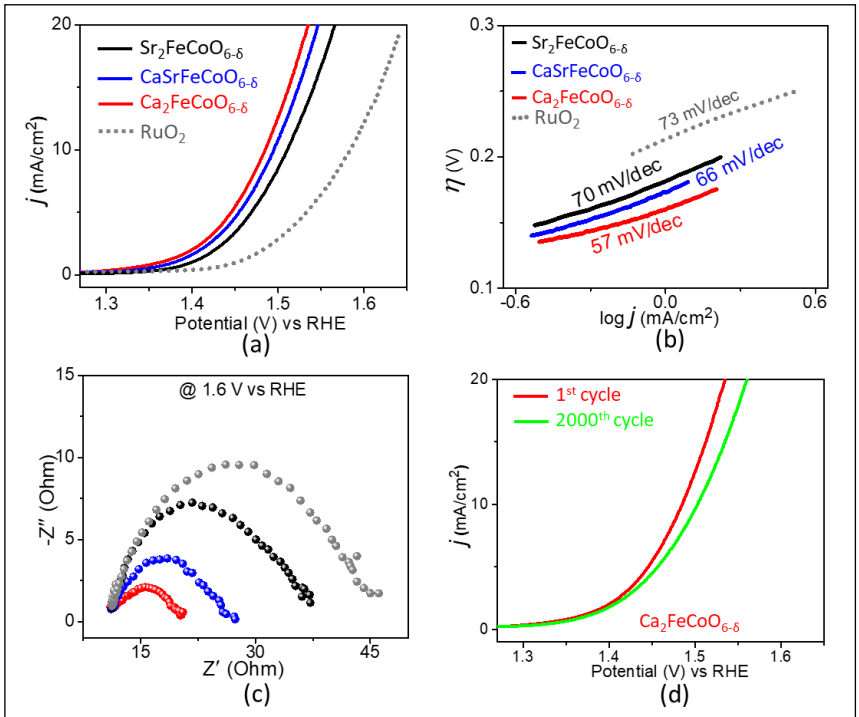

Figure 3. (a) OER polarization curves in 1M KOH. (b) Tafel plots and slopes. (c) Impedance spectroscopy data indicating the charge transfer resistance in the OER region. (d) Polarization curve for $Ca_2FeCoO_{6-\delta}$ after 2000 cycles.

foam, obtained from a metal-organic framework.[28] Another example is the reduced necklace-like multishelled hollow structure of a spinel transition-metal oxide, obtained using sacrificial templates of carbonaceous microspheres, which leads to an overpotential of η_{10} = 240 mV.[29] Catalysts with ultrahigh activity that can be used in bulk form, without intricate nanofabrication or multicomponent composite formation are rare.

The trend in the OER kinetics, evident from the Tafel slopes (Figure 3b), and the charge-transfer resistance, from impedance spectroscopy (Figure 3c), match the trend of the electrocatalytic activity. Importantly, the best catalyst, $Ca_2FeCoO_{6-\delta}$, is highly stable and retains its high catalytic activity for at least 2000 cycles, as shown in Figure 3d. In addition, the structural integrity and transition metal oxidation states are maintained, as demonstrated by X-ray diffraction and X-ray photoelectron spectroscopy (XPS) experiments before and after 2000 cycles (Figures 4).

To explore the effect of structural order in more depth, we conducted density functional theory (DFT) calculations on the disordered material $Sr_2FeCoO_{6-\delta}$, as well as the highly ordered compound $Ca_2FeCoO_{6-\delta}$ (Figure 5). These calculations indicate that the structural order leads to a methodical shift of centers of the transition-metal *d*-bands and oxygen *p*-band toward the Fermi level. For the disordered system $Sr_2FeCoO_{6-\delta}$, the centers of the bands are at -4.885 eV (Fe *d*), -4.446 eV (Co *d*), and -2.417 eV (O *p*). On the other hand, DFT calculations for the ordered material $Ca_2FeCoO_{6-\delta}$ show a shift toward the Fermi level, leading to band center energies of -4.403 eV (Fe *d*), -3.713 eV (Co *d*), and -2.215 eV (O *p*). It has been previously proposed that the shift in the center of the *d*-band toward the Fermi level can result in enhanced interactions with the OER intermediates,[30, 31] leading to an improvement in the electrocatalytic activity. A further outcome of the structural order, indicated by DFT calculations, is a greater proximity of the centers of the transition-metal *d*-bands to the oxygen *p*-band for $Ca_2FeCoO_{6-\delta}$ as compared to $Sr_2FeCoO_{6-\delta}$. Some researchers have suggested that this proximity leads to enhanced covalency and a greater degree of *p*-character of the transition metal *d* bands, resulting in better charge-transfer between the catalyst and the oxygen-containing intermediates.[32] Therefore, in transition from a disordered system to an ordered structure, the combined effect of the shift of the band centers toward the Fermi level and the enhanced proximity of the centers of the metal *d* and oxygen *p* bands can contribute to the remarkable enhancement of the electrocatalytic activity.

To further demonstrate the impact of structural order, we conducted additional DFT calcula-

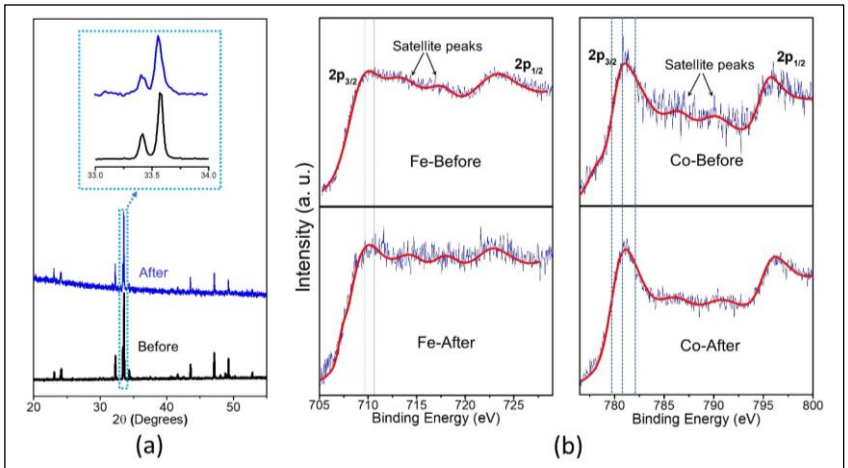

Figure 4. (a) X-ray diffraction and (b) XPS, before and after 2000 cycles of OER for $Ca_2FeCoO_{6-\delta}$.

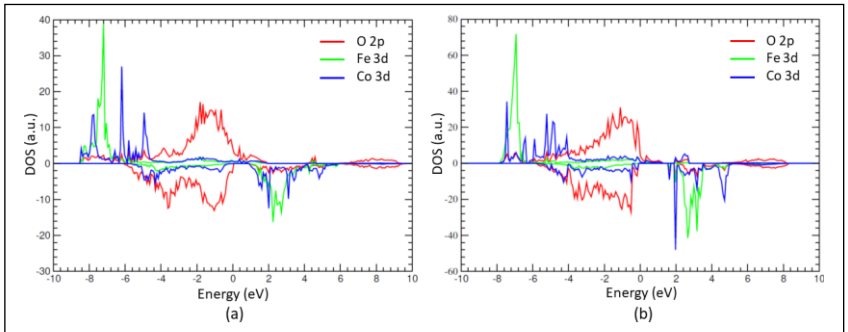

Figure 5. Density of States (DOS) with spin up (above zero) and down (below zero) from DFT calculations on (a) disordered $Sr_2FeCoO_{6-\delta}$, and (b) ordered $Ca_2FeCoO_{6-\delta}$. Fermi level is shifted to zero.

tions (Figure S4) for $Ca_2FeCoO_{6-\delta}$ using a hypothetical disordered model. The hypothetical structure was similar to that of $Sr_2FeCoO_{6-\delta}$, but contained calcium instead of strontium. The simulations indicated that a hypothetical disordered structure for $Ca_2FeCoO_{6-\delta}$ would have lower band center energies, -5.2023 eV (Fe *d*) and -4.3388 eV (Co *d*), compared to those of the real, ordered structure of $Ca_2FeCoO_{6-\delta}$. These findings indicate that a disordered structure, whether containing Sr or Ca, consistently has lower band energies than the ordered structure. These calculations underline the crucial impact of structural order in modifying the electronic structure and the subsequent enhancement of the electrocatalytic performance.

In summary, we have shown a remarkably high electrocatalytic performance, achieved through a systematic increase in the degree of ordering of oxygen-vacancies. This approach leads to a remarkably low overpotential for an oxide catalyst, which can be used in bulk form, without the need for elaborate nanofabrication, multicomponent composite formation, or any additional processing. We propose that the modification of the ordering schemes of oxygen-vacancies can be used as a tool for the design of highly active oxide electrocatalysts for water electrolysis.

ASSOCIATED CONTENT

Supporting Information

The Supporting Information is available free of charge on the ACS Publications website.
Experimental and computational methods, Rietveld refinement profiles, scanning electron microscopy data, cyclic voltammetry plots in non-Faradaic region, calculated density of states for a hypothetical model, and tables of refined structural parameters.

ACKNOWLEDGMENT

This work is supported by the National Science Foundation (NSF) under grant no. DMR-1943085. M. Y. acknowledges the computing resource support from the Cardinal Research Cluster at the University of Louisville.

REFERENCES

1. Suntivich, J.; May, K. J.; Gasteiger, H. A.; Goodenough, J. B.; Shao-Horn, Y., A Perovskite Oxide Optimized for Oxygen Evolution Catalysis from Molecular Orbital Principles. *Science* **2011,** *334*, 1383.
2. Zhu, Y.; Zhou, W.; Chen, Z. G.; Chen, Y.; Su, C.; Tade, M. O.; Shao, Z., $SrNb_{0.1}Co_{0.7}Fe_{0.2}O_{3-\delta}$ Perovskite as a Next-Generation Electrocatalyst for Oxygen Evolution in Alkaline Solution. *Angew. Chem., Int. Ed.* **2015,** *54*, 3897.
3. Su, C.; Wang, W.; Chen, Y.; Yang, G.; Xu, X.; Tadé, M. O.; Shao, Z., $SrCo_{0.9}Ti_{0.1}O_{3-\delta}$ As a New Electrocatalyst for the Oxygen Evolution Reaction in Alkaline Electrolyte with Stable Performance. *ACS Appl. Mater. Interfaces* **2015,** *7*, 17663-17670.
4. Park, H. W.; Lee, D. U.; Zamani, P.; Seo, M. H.; Nazar, L. F.; Chen, Z., Electrospun porous nanorod perovskite oxide/nitrogen-doped graphene composite as a bi-functional catalyst for metal air batteries. *Nano Energy* **2014,** *10*, 192-200.
5. Jung, J.-I.; Risch, M.; Park, S.; Kim, M. G.; Nam, G.; Jeong, H.-Y.; Shao-Horn, Y.; Cho, J., Optimizing nanoparticle perovskite for bifunctional oxygen electrocatalysis. *Energy Environ. Sci.* **2016,** *9*, 176-183.
6. Tian, S.; He, J.; Huang, H.; Song, T.-s.; Wu, X.; Xie, J.; Zhou, W., Perovskite-Based Multifunctional Cathode with Simultaneous Supplementation of Substrates and Electrons for Enhanced Microbial Electrosynthesis of Organics. *ACS Appl. Mater. Interfaces* **2020,** *12*, 30449-30456.
7. Zhu, Y.; Zhou, W.; Zhong, Y.; Bu, Y.; Chen, X.; Zhong, Q.; Liu, M.; Shao, Z., A Perovskite Nanorod as Bifunctional Electrocatalyst for Overall Water Splitting. *Adv. Energy Mater.* **2017,** *7*, 1602122.
8. Hona, R. K.; Karki, S. B.; Cao, T.; Mishra, R.; Sterbinsky, G. E.; Ramezanipour, F., Sustainable Oxide Electrocatalyst for Hydrogen and Oxygen-Evolution Reactions. *ACS Catal.* **2021,** *11*, 14605−14614.
9. Hona, R. K.; Ramezanipour, F., Remarkable Oxygen-Evolution Activity of a Perovskite Oxide from the $Ca_{2-x}Sr_xFe_2O_{6-\delta}$ Series. *Angew. Chem.* **2019,** *58*, 2060-2063.
10. Hona, R. K.; Huq, A.; Ramezanipour, F., Unraveling the Role of Structural Order in the Transformation of Electrical Conductivity in $Ca_2FeCoO_{6-\delta}$, $CaSrFeCoO_{6-\delta}$, and $Sr_2FeCoO_{6-\delta}$. *Inorg. Chem.* **2017,** *56*, 14494-14505.
11. Matsumoto, Y.; Sato, E., Electrocatalytic properties of transition metal oxides for oxygen evolution reaction. *Mater. Chem. Phys.* **1986,** *14*, 397-426.
12. McCrory, C. C. L.; Jung, S.; Peters, J. C.; Jaramillo, T. F., Benchmarking Heterogeneous Electrocatalysts for the Oxygen Evolution Reaction. *J. Am. Chem. Soc.* **2013,** *135*, 16977-16987.
13. Li, X.; He, L.; Zhong, X.; Zhang, J.; Luo, S.; Yi, W.; Zhang, L.; Hu, M.; Tang, J.; Zhou, X.; Zhao, X.; Xu, B., Evaluation of A-Site Ba^{2+}-Deficient $Ba_{1-x}Co_{0.4}Fe_{0.4}Zr_{0.1}Y_{0.1}O_{3-\delta}$ Oxides as Electrocatalysts for

Efficient Hydrogen Evolution Reaction. *Scanning* **2018,** *2018*, 1341608-1341608.
14. Ji, D.; Liu, C.; Yao, Y.; Luo, L.; Wang, W.; Chen, Z., Cerium substitution in $LaCoO_3$ perovskite oxide as bifunctional electrocatalysts for hydrogen and oxygen evolution reactions. *Nanoscale* **2021,** *13*, 9952-9959.
15. Wang, J.; Gao, Y.; Chen, D.; Liu, J.; Zhang, Z.; Shao, Z.; Ciucci, F., Water Splitting with an Enhanced Bifunctional Double Perovskite. *ACS Catal.* **2018,** *8*, 364-371.
16. Pan, Y.; Chen, Y.; Li, X.; Liu, Y.; Liu, C., Nanostructured nickel sulfides: phase evolution, characterization and electrocatalytic properties for the hydrogen evolution reaction. *RSC Adv.* **2015,** *5*, 104740-104749.
17. Oh, S.; Kim, H.; Kwon, Y.; Kim, M.; Cho, E.; Kwon, H., Porous Co–P foam as an efficient bifunctional electrocatalyst for hydrogen and oxygen evolution reactions. *J. Mater. Chem. A* **2016,** *4*, 18272-18277.
18. Song, F.; Hu, X., Ultrathin Cobalt–Manganese Layered Double Hydroxide Is an Efficient Oxygen Evolution Catalyst. *J. Am. Chem. Soc.* **2014,** *136*, 16481-16484.
19. Moir, J.; Soheilnia, N.; O'Brien, P.; Jelle, A.; Grozea, C. M.; Faulkner, D.; Helander, M. G.; Ozin, G. A., Enhanced Hematite Water Electrolysis Using a 3D Antimony-Doped Tin Oxide Electrode. *ACS Nano* **2013,** *7*, 4261-4274.
20. Tahir, M.; Pan, L.; Zhang, R.; Wang, Y.-C.; Shen, G.; Aslam, I.; Qadeer, M. A.; Mahmood, N.; Xu, W.; Wang, L.; Zhang, X.; Zou, J.-J., High-Valence-State NiO/Co_3O_4 Nanoparticles on Nitrogen-Doped Carbon for Oxygen Evolution at Low Overpotential. *ACS Energy Lett.* **2017,** *2*, 2177-2182.
21. Fan, Z.; Liao, F.; Shi, H.; Liu, Y.; Shao, M.; Kang, Z., Highly efficient water splitting over a RuO_2/F-doped graphene electrocatalyst with ultra-low ruthenium content. *Inorg. Chem. Front.* **2020,** *7*, 2188-2194.
22. Das, D.; Nanda, K. K., One-step, integrated fabrication of Co_2P nanoparticles encapsulated N, P dual-doped CNTs for highly advanced total water splitting. *Nano Energy* **2016,** *30*, 303-311.
23. Tang, L.; Fan, T.; Chen, Z.; Tian, J.; Guo, H.; Peng, M.; Zuo, F.; Fu, X.; Li, M.; Bu, Y.; Luo, Y.; Li, J.; Sun, Y., Binary-dopant promoted lattice oxygen participation in OER on cobaltate electrocatalyst. *Chem. Eng. J.* **2021,** *417*, 129324.
24. Miao, X.; Wu, L.; Lin, Y.; Yuan, X.; Zhao, J.; Yan, W.; Zhou, S.; Shi, L., The role of oxygen vacancies in water oxidation for perovskite cobalt oxide electrocatalysts: are more better? *Chem. Commun.* **2019,** *55*, 1442-1445.
25. Wu, Z.; Sun, L.-P.; Xia, T.; Huo, L.-H.; Zhao, H.; Rougier, A.; Grenier, J.-C., Effect of Sr doping on the electrochemical properties of bi-functional oxygen electrode $PrBa_{1-x}Sr_xCo_2O_{5+\delta}$. *J. Power Sources* **2016,** *334*, 86-93.
26. Guo, Q.; Li, X.; Wei, H.; Liu, Y.; Li, L.; Yang, X.; Zhang, X.; Liu, H.; Lu, Z., Sr, Fe Co-doped Perovskite Oxides With High Performance for Oxygen Evolution Reaction. *Front. Chem.* **2019,** *7*, 224.
27. Wang, X.; Yu, L.; Guan, B. Y.; Song, S.; Lou, X. W., Metal–Organic Framework Hybrid-Assisted Formation of Co_3O_4/Co-Fe Oxide Double-Shelled Nanoboxes for Enhanced Oxygen Evolution. *Adv. Mater.* **2018,** *30*, 1801211.
28. Lu, X.-F.; Gu, L.-F.; Wang, J.-W.; Wu, J.-X.; Liao, P.-Q.; Li, G.-R., Bimetal-Organic Framework Derived $CoFe_2O_4$/C Porous Hybrid Nanorod Arrays as High-Performance Electrocatalysts for Oxygen Evolution Reaction. *Adv. Mater.* **2017,** *29*, 1604437.
29. Peng, S.; Gong, F.; Li, L.; Yu, D.; Ji, D.; Zhang, T.; Hu, Z.; Zhang, Z.; Chou, S.; Du, Y.; Ramakrishna, S., Necklace-like Multishelled Hollow Spinel Oxides with Oxygen Vacancies for Efficient Water Electrolysis. *J. Am. Chem. Soc.* **2018,** *140*, 13644-13653.
30. Sun, Y.; Zhao, Z.; Wu, S.; Li, W.; Wu, B.; Liu, G.; Chen, G.; Xu, B.; Kang, B.; Li, Y.; Li, C., Engineering of the d-Band Center of Perovskite Cobaltite for Enhanced Electrocatalytic Oxygen Evolution. *ChemSusChem* **2020,** *13*, 2671-2676.
31. Sun, S.; Zhou, X.; Cong, B.; Hong, W.; Chen, G., Tailoring the d-Band Centers Endows $(Ni_xFe_{1-x})_2P$ Nanosheets with Efficient Oxygen Evolution Catalysis. *ACS Catal.* **2020,** *10*, 9086-9097.
32. Song, J.; Wei, C.; Huang, Z.-F.; Liu, C.; Zeng, L.; Wang, X.; Xu, Z. J., A review on fundamentals for designing oxygen evolution electrocatalysts. *Chem. Soc. Rev.* **2020,** *49*, 2196-2214.

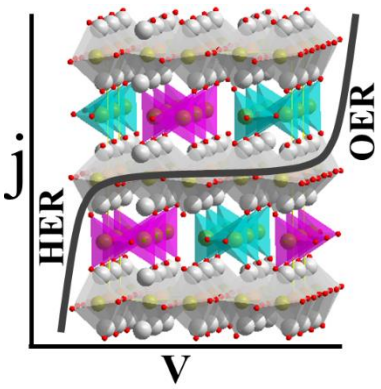
j
HER
OER
V